NANO LETTERS

2009
Vol. 9, No. 2
738-744

Mechanism and Kinetics of Growth Termination in Controlled Chemical Vapor Deposition Growth of Multiwall Carbon Nanotube Arrays

Michael Stadermann,[†] Sarah P. Sherlock,[†] Jung-Bin In,[†,§] Francesco Fornasiero,[†] Hyung Gyu Park,[†,‡,§] Alexander B. Artyukhin,[†] Yinmin Wang,[†] James J. De Yoreo,[||] Costas P. Grigoropoulos,[§] Olgica Bakajin,[†,⊥] Alexander A. Chernov,[†] and Aleksandr Noy*[,†,#]

Physical and Life Sciences Directorate, Lawrence Livermore National Laboratory, Livermore, California 94550, Engineering Directorate, Lawrence Livermore National Laboratory, Livermore, California 94550, Department of Mechanical Engineering, University of California, Berkeley, Berkeley, California 94720, The Molecular Foundry, Lawrence Berkeley National Laboratory, Berkeley, California 94720, Center for Biophotonics Science and Technology, University of California, Davis, Sacramento, California 95616, and School of Natural Sciences, University of California, Merced, Merced, California 95344

Received October 30, 2008; Revised Manuscript Received November 26, 2008

ABSTRACT

We have investigated growth kinetics of multiwall carbon nanotube (MWCNT) arrays produced by catalytic thermal decomposition of ethylene gas in hydrogen, water, and argon mixture. The MWCNT growth rate exhibits a nonmonotonic dependence on total pressure and reaches a maximum at ~750 Torr of total pressure. Water concentrations in excess of 3000 ppm lead to the decrease in the observed growth rate. Optimal pressure and water concentration combination results in a reliable growth of well-aligned MWCNT arrays at a maximum growth rate of ~30 μm/min. These MWCNT arrays can reach heights of up to 1 mm with typical standard deviations for the array height of less than 8% over a large number of process runs spread over the time of 8 months. Nanotube growth rate in this optimal growth region remains essentially constant until growth reaches an abrupt and irreversible termination. We present a quantitative model that shows how accumulation of the amorphous carbon patches at the catalyst particle surface and the carbon diffusion to the growing nanotube perimeter causes this abrupt growth cessation. The influence of the partial pressures of ethylene and hydrogen on the ethylene decomposition driving force explains the nonlinear behavior of the growth rate as a function of total process pressure.

Vertically aligned carbon nanotube (CNT) arrays promise widespread use in a variety of applications ranging from field emission cathodes[1] and supercapacitors[2] to gas chromatography columns[3] and nanoelectronic devices, to sensors[4] and nanofiltration membranes.[5,6] Catalytic CVD growth, in which a mixture of the carbon feedstock gases flows over the metal nanoparticle catalyst at high temperatures,[7] readily produces such arrays in laboratory conditions.[1] However, growth mechanisms and, in particular growth termination mechanisms, are still poorly understood.[4,8] As the result, synthetic control over nanotube diameter, chirality, and length is either limited or nonexistent.

Researchers have reported numerous process parameters such as feed gas mixture composition and flow rate, growth temperature, reaction pressure, catalyst composition, and annealing conditions[7,9−13] that can dramatically change the yield of the nanotube arrays and quality of the carbon nanotubes. Despite these studies, in many instances it is still difficult to achieve reproducible nanotube array growth even when using identical process parameters. These problems can partially explain limited use of aligned CNT arrays in real-world applications as well as point to the reason why only a few kinetic studies of nanotube growth exist to date.[8,14,15]

* Corresponding author, noy1@llnl.gov.
[†] Physical and Life Sciences Directorate, Lawrence Livermore National Laboratory.
[‡] Engineering Directorate, Lawrence Livermore National Laboratory.
[§] Department of Mechanical Engineering, University of California, Berkeley.
[||] The Molecular Foundry, Lawrence Berkeley National Laboratory.
[⊥] Center for Biophotonics Science and Technology, University of California, Davis.
[#] School of Natural Sciences, University of California, Merced.

10.1021/nl803277g CCC: $40.75
Published on Web 01/15/2009

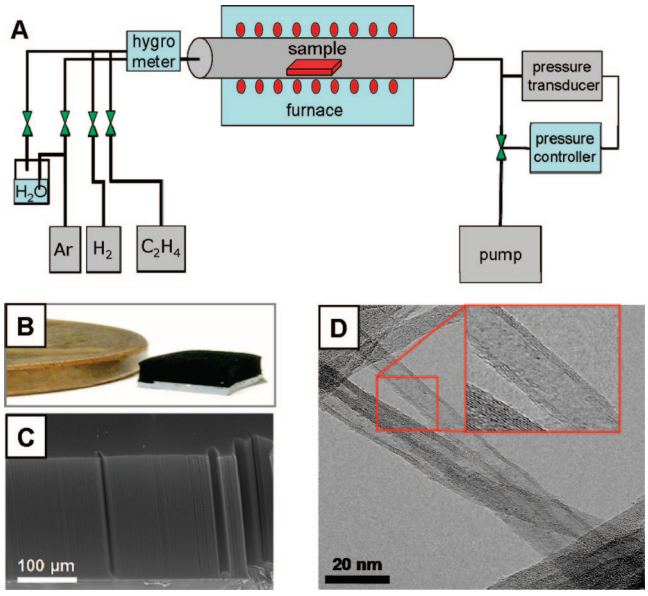

Figure 1. Carbon nanotube array growth and characterization. (A) Schematic of the CVD growth setup. Mass flow controllers set the flow of all process gases to the system. A hygrometer controls the water content of the gas mixture before it enters the furnace, and the pressure at which the reaction takes place is controlled at the exhaust end. (B) A photograph showing a tall MWNT film on a silicon substrate next to a penny coin. (C) SEM image of the nanotube mat grown at 750 °C, 760 Torr, 2000 ppm of water for 10 min. (D) TEM image of the MWNTs grown at the same conditions as the array in (B).

In this work we investigated the growth efficiency and growth kinetics for vertically aligned CNT array growth on silicon substrates. We present the data that show that variations in growth conditions have a substantial effect on the CNT array growth rates. We then discuss the mechanistic basis for the observed effects and propose a model that reproduces most of the features of the observed growth kinetics.

Materials and Methods. Carbon nanotube growth experiments were performed in a 1 in. tube furnace (Lindberg Blue TF55035A) modified for control over the process pressure and water content of the feed gas (Figure 1A). All of our studies were performed using ethylene as our carbon source. The feed gas mixture always had 30% argon, 20% hydrogen, and 50% ethylene, while total flow rates varied from 100 to 2000 sccm. To add water to the gas mixture, we split the argon line into two streams, pass one of the streams through a water bubbler, and then adjust the splitting ratio so that mixing wet argon and dry argon produces the desired humidity while retaining a total argon fraction of 30%. The water content of the feed gas was measured with a hygrometer at the furnace entrance. We find that the hygrometer is essential for obtaining reproducible water concentrations; simply controlling the temperature of the bubbler and mixing the same amount of wet argon to the gas mixture does not yield reproducible water concentrations due to a gradual drying of the gas lines. Our system uses two hygrometers, a Nyad Inc. model 160 and a Bartec Hygrophil F5672. The first hygrometer equilibrates much faster than the other one but is prone to decalibrating over time. The Hygrophil F5672 gives consistent readings but takes a relatively long time to equilibrate. By using the "slow" hygrometer to provide a reference for the "fast" hygrometer, we can control the humidity in real time while still having an accurate overall humidity value. We controlled the process pressure with a custom-built feedback system consisting of manometer, control valve, and pressure controller placed at the exhaust end of the furnace (calculated error in the pressure determination due to the hydrodynamic resistance of the piping between the manometer and the reaction chamber is less than 0.01%). This system holds constant pressure to within 0.2 Torr accuracy, over the 100−1000 Torr range.

Our nanotube growth catalyst consists of 10 nm Al and 3 nm Fe films deposited onto the surface of a Si wafer with native oxide by e-beam evaporation. Before growth, the samples were oxidized in air at 500 °C for 15 min. Then the temperature was ramped up at 40 °C/min to 750 °C while flowing argon and hydrogen and held at 750 °C for 12 min before adding ethylene. The water is adjusted after the sample annealed for 2 min at 750 °C. The growth was timed from the moment the mass flow controller was opened. We measured the height of the tall forests (higher than 60 μm) with an optical microscope; shorter arrays were characterized by imaging the array cross section with a Hitachi S-800 scanning electron microscope.

Raman spectra were collected with Nicolet Almega XR dispersive micro-Raman spectrometer using 473 and 633 nm excitation length and 100× collection objective. Scanning electron microscopy (SEM) images were obtained using JEOL 7401F and Hitachi S800 scanning electron microscopes. Transmission electron microscopy (TEM) images were recorded on a Philips CM300-FEG TEM operated at 300 kV and equipped with a Gatan image filter system. The extraction voltage for the field-emission gun was 4.2 keV. The spatial resolution of the microscope is approximately 1.8 Å.

CNT Array Growth Yield. When we performed systematic variation of total gas pressure and water concentration in our chemical vapor deposition (CVD) system (Figure 1A), we found that they resulted in the large variations in the height of the CNT arrays produced after 10 min of growth. This height value reaches a maximum as functions of the total pressure at ~700 Torr. Water concentration above ~2500 ppm diminishes the growth rate. Remarkably, we found a very stable region around 760 Torr of total process pressure and 1500 ppm H_2O content that maximizes the CNT growth rate (Figure 2) and routinely and reproducibly produces carbon nanotube arrays (Figure 1B,C) of up to 1 mm in height. The water/ethylene ratio in this region is 1/330, which curiously is within a factor of 3 of the optimal water/ethylene ratio previously reported by Futaba et al. for growth of single-wall carbon nanotube (SWNT) arrays.[14] Qualitatively, the observed sensitivity of the CNT growth to the feed gas pressure and water concentration is not surprising, since the total pressure affects the partial pressures of the reaction species and, thus, ultimately determines the incoming flux of carbon to the catalyst. The primary role of the water is assumed to oxidize and remove amorphous carbon

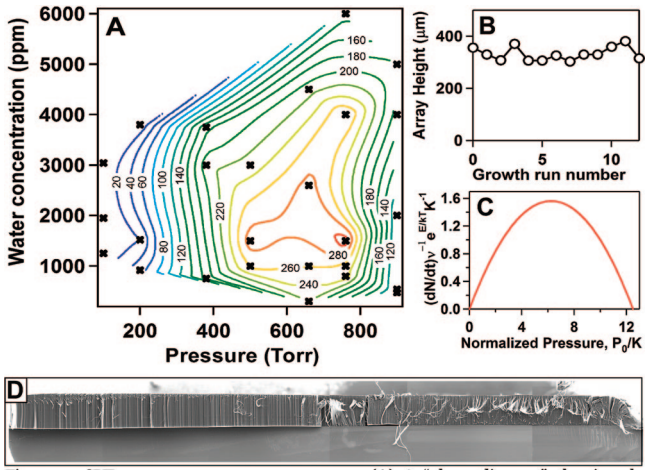

Figure 2. CVD process parameter space. (A) A "phase diagram" showing the nanotube array height measured after 10 min of growth as a function of water concentration and total process pressure. All growth runs were performed at 750 °C. The crosses mark the points in the parameter space where measurements were performed. The topographical lines are extrapolated and serve to guide the eye. The numbers on the topographical lines are array heights in micrometers. (B) Plot of measured CNT array height obtained in 13 growth runs using identical growth parameters and spaced over an 8 month period. (C) Plot of the predicted normalized rate of pyrolyzed carbon (CNT growth precursor) production predicted by eq 10 as a function of the normalized total process pressure. (D) SEM micrograph of a cross section of ~350 μm tall CNT array on the Si substrate demonstrating growth uniformity over large scale.

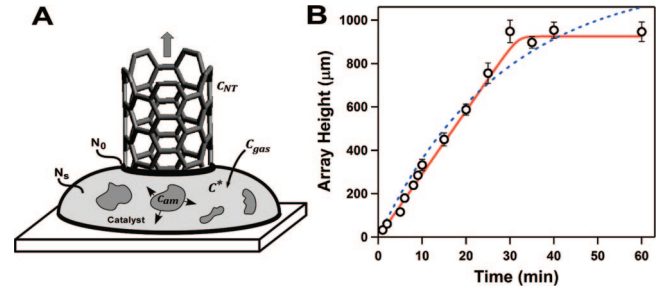

Figure 3. Mechanism and kinetics of growth termination. (A) Schematics of the poisoning/diffusion model of carbon nanotube growth termination. Growth proceeds through a two-stage process that involves conversion of the gas-phase precursor C_{gas} to an activated surface-bound form, C*. C* can then diffuse through the catalyst particle and incorporate into a growing nanotube, or form amorphous carbon patches C_{am} that block the catalyst particle surface. The figure also indicates various concentration of the carbon atoms used in the model description. Note that the catalyst particle shown in this figure is used as only as a simplified representation and does not reflect the true geometry of the catalyst/CNT system. (B) Plot of the measured nanotube array height (open circles) as a function of the growth time. Each data point represents an average of at least three individual growth runs. The red solid line corresponds to the best fit to eqs 6 and 7 using the calculated value of $G_D = 2.2 \times 10^5$ μm/min; the parameters producing the best fit were $G_0 = 30.7$ μm/min, $\tau = 14.5$ min. The dotted blue line is the best fit to the data using the exponential growth model by Iijima and co-workers.[14]

on the catalyst, along with etching the graphitic carbon, which could also have drastic effects on the CNT growth.[16]

The height of the CNT arrays grown at the optimal conditions in our system was extremely uniform and varied by only 1−2% over the sample (Figures 1C and 2D). The data were highly reproducible from run to run: nanotube array height measured after 13 different 10 min long growth runs over the course of 8 months using three different catalyst depositions showed standard deviation of only 7.8% (Figure 2B). The TEM analysis indicates that growth in the optimal region of the parameter space produces multiwall carbon nanotubes (MWNTs) with well-graphitized sidewalls and low concentration of defects (Figure 1D).

Outside the optimal growth plateau region the growth rate drops quickly (Figure 2A). In general, the growth rate shows a stronger dependence on pressure than on water content, especially in the high pressure region; although water content variations alone could produce up to 50% difference in growth height. The strong growth rate dependence on pressure, away from the dome top in Figure 2A, suggests that even day-to-day atmospheric pressure fluctuations can lead to significant height changes. This observation might explain why some recipes found in literature for growth at ambient pressures yield inconsistent results.

CNT Arrays Growth Kinetics. To gain insight into the microscopic mechanism of the CVD growth at the optimal conditions, we have studied growth kinetics by terminating the reaction at different growth times. Since our growth was very reproducible from run to run, this method allowed us to obtain a highly accurate kinetic curve (Figure 3B). Our data show that growth of MWNT in the optimal regime does not follow an exponential growth kinetics reported in several other studies.[8,14] Instead, the growth proceeds at constant rate, where the array height increases linearly with time, and then abruptly terminates as the array reaches its maximum height value. A similar abrupt termination kinetics was also reported recently by other research groups.[15,17] All of our growth runs indicate that the catalyst remains on the bottom of the sample during the growth process. Indeed, the backscatter-electron imaging with SEM showed no metal particles at the top of the array and the catalyst particles were found remaining at the substrate after mechanical removal of the nanotube array. If the growth process was terminated before the system entered the growth height plateau region, the nanotube growth could be restarted, albeit at an overall reduced rate (see Figure S3 in Supporting Information). In contrast, once the growth stopped it could not be resumed. Clearly, these data contradict the commonly used exponential growth decay model that assumes monotonic decrease in catalyst activity over time.[14] We have also noticed significant edge effects (i.e., array edges being higher or lower than the center region) for the arrays grown at nonoptimal conditions (see Figure S1a,b, Supporting Information). Curiously, these effects are virtually absent for the arrays grown at the optimal conditions where we observed extremely uniform edge-to-edge array thickness (Figure 2c).

CNT Growth Cessation. The growth cessation may be caused either by poisoning of the catalyst, or of the carbon nanotube's growth front, or by limitations imposed by diffusion of carbon feedstock to the catalyst surface through

the dense array of CNTs. Maruyama and co-workers recently analyzed the feedstock diffusion limitations in the CNT growth process[18] and found that for MWNT growth the diffusion does not limit the growth kinetics until the arrays grow to the lengths that are more than an order of magnitude higher than arrays obtained in our study. Also, the growth rate limited by gas diffusion to/from the catalyst particle down through the CNT array of height H_g should decrease as $1/H_g$, i.e., much more gradually than that observed in our experiments. High-resolution SEM images show that before the growth cessation, nanotubes emerging from Fe catalyst particles lose their general alignment and become randomly oriented over several micrometers near the substrate (Figure S2 in the Supporting Information). This behavior suggests a spatial growth instability that hardly could be ascribed to poisoning of the perimeter of the growing nanotube, since poisoning particles are usually irreversibly attached to the interface that they poison;[19] therefore poisoning of the growing end of a nanotube is also unlikely.

Thus, we conclude that the catalyst poisoning is the most probable cause for the growth cessation. Most likely the poisoning species is amorphous carbon. First, the presence of water vapor that etches amorphous carbon leads to an substantial enhancement of the nanotube growth yield.[20] Second, micro-Raman spectroscopy mapping (see Figure S1 in the Supporting Information) revealed that the G/D band intensity ratio has continuously decreased during the array growth, indicating increasing concentration of amorphous carbon near the catalyst surface species at the end of the growth process (G-band Raman signal typically indicates the level of graphitized carbon, while D-band corresponds to disordered amorphous carbon).

What is the mechanism of the growth poisoning? We first describe a qualitative model that accounts for the kinetic features observed in our growth experiments. We postulate that carbon nanotube growth proceeds in two stages. At first the ethylene molecule adsorbs on the surface of the catalyst particle and is ultimately converted into a carbon atom C, which can diffuse to the catalyst particle step edge and incorporate into a nanotube.[21,22] Alternatively, it may nucleate a new amorphous carbon cluster or join an already existing one (Figure 3A). These cluster patches eventually grow to cover the surface of the catalyst particle thus blocking the ethylene decomposition and carbon supply to the nanotube. This mechanism explains irreversible growth cessation. Indeed, Ajayan and co-workers reported that after the 10 min of high-temperature oxidation, the catalyst activity resumes, and a second nanotube array may be grown on the same substrate, while further oxidation may detach the array sandwich from the substrate. Probably, this harsh oxidation removes the amorphous carbon film along with the curved defect-rich nanotube portions, and reactivates the catalyst.[23] Additionally, we expect that when the carbon patches cover the catalyst particle surface almost completely, the feeding of the growing nanotube perimeter becomes spatially asymmetric and varying in time. That asymmetry changes the tube orientation and induces the increased entanglement observed in the last stages of the array growth (Figure S2, Supporting Information).

We now use this model to construct a semiquantitative description of the growth and poisoning kinetics. According to the classical Kolmogorov−Johnson−Mehl−Avrami (KJMA) theory,[19,24−26] the fraction, $g(t)$, of the surface not yet covered by the passivating patches by the time t after the start of the deposition is given by

$$g(t) = \exp\left[-\frac{\pi J V^2 t^3}{3}\right] \quad (1)$$

The KJMA theory is strictly applicable if the total size of the system is much larger than the distance between the (round) patches, and a more exact description would include a correction for the finite size of the surface. Our derivation is based on a simple KJMA model (eq 1), and therefore it should be considered as an approximation. The overall carbon nanotube growth rate v_g would be proportional to the open surface area of the catalyst

$$v_g = v_0 g(t) = v_0 \exp\left[-\frac{\pi J V^2 t^3}{3}\right] \quad (2)$$

where J (1/(m^2 s)) is the rate of the amorphous carbon nucleation, V (m/s) is the linear expansion rate of a patch, and v_0 (m/s) is the nanotube growth rate on a clean catalyst. The parameter v_0 is controlled by the delivery of the carbon atoms to the growing nanotube perimeter and incorporation rate, and we can estimate it using the model of Tibbetts et al.[27] Briefly, this model postulates that carbon species adsorb from the gas phase onto the surface of the catalyst particle and creates a carbon concentration on the surface that is highly supersaturated with respect to the carbon concentration at the perimeter of the growing carbon nanotube. Concentration gradient then leads the carbon atoms to diffuse through the iron particle and incorporate into the nanotube. Although the real geometry of the catalyst particle and a growing carbon nanotubes is complicated, we follow Tibbetts and coworkers by modeling the catalyst particle as a cylinder of radius and thickness equal to the outer radius of the carbon nanotube R_0. Under these assumptions, the growth rate v_g is

$$v_g = \frac{J_s \Omega}{1 - \left(\frac{r_i}{r_o}\right)^2} \frac{N_s - N_0}{N_s} \frac{1}{1 + \frac{J_s R}{D N_s}} \quad (3)$$

Here J_s (1/(m^2 s)) is the effective incoming flux of carbon atoms that accounts for ethylene adsorption, its thermal decomposition that produces carbon on the catalyst−gas interface, and hydrogen release back to the gas phase, along with inverse reactions that produce volatile hydrocarbons from adsorbed C and gaseous hydrogen. Finally, J_s includes an energy barrier that C atoms must overcome to dissolve in the solid Fe−C catalyst (likely austenite). N_s (1/m^3) is the bulk concentration of mobile carbon atoms in the catalyst just below its interface, and N_0 is the carbon atom concentration in equilibrium with the perimeter of the growing carbon nanotube (this concentration could also include contributions from carbon atoms delivered by surface diffusion). The $2r_o$ and $2r_i$ are the outer and inner diameters of the carbon nanotube, D is the effective diffusivity of carbon atoms that accounts for both bulk and surface diffusion over the effective distance R of the order of the catalyst radius, and Ω is the volume of a carbon atom in graphite.

The ratio J_sR/DN_s defines the ratio of the carbon production rate J_s to the carbon diffusion rate. Precipitation of amorphous carbon observed in the Raman spectroscopy data, along with nanotube graphite, suggests that supersaturation of carbon in the catalyst particle and on the catalyst surface is high enough to drive the growth process. Therefore, it is reasonable to assume that $N_s \gg N_0$. That assumption simplifies eq 3 to:

$$v_g = \frac{J_s\Omega}{1-\left(\frac{r_i}{r_o}\right)^2}\frac{1}{1+\frac{J_sR}{DN_s}} \quad (4)$$

The impact of amorphous carbon patches formation manifests itself as the reduction of the catalyst surface area where the carbon is produced from ethylene while the concentration of carbon on the still poison-free surface does not change. Then, the *average* carbon concentration over the whole catalyst interface will be

$$N_s(t) = N_s{}^0 g(t) = N_s{}^0 \exp\left[-\frac{t^3}{\tau^3}\right] \quad (5)$$

where $N_s{}^o$ is the carbon concentration on a clean catalyst particle and τ is the characteristic poisoning time $\tau = (3/\pi JV^2)^{1/3}$. We now can combine eqs 2, 4, and 5 into a simple expression

$$v_g = \frac{G_0}{1+\frac{G_0}{G_D}\exp\left[\frac{t^3}{\tau^3}\right]} \quad (6)$$

where

$$G_0 = \frac{J_s\Omega}{1-(r_i/r_o)^2}$$

and

$$G_D = \frac{D\Omega N_s{}^0}{R[1-(r_i/r_o)^2]}$$

Finally, the observed height H_g of the carbon nanotube array is

$$H_g = \int_0^t v_g(t)\,dt \quad (7)$$

Equation 6 contains three parameters: characteristic poisoning time, τ, the growth rate G_0 on the clean catalyst at the infinitely fast diffusion, and the growth rate G_D, also on a clean catalyst, but fully controlled by slow diffusion (i.e., growth rate at an infinitely fast supply of carbon). Note that at least initially the diffusion through the catalyst particle should not limit the growth speed, i.e., $G_D \gg G_0$.

We can estimate G_D by assuming that we can approximate the value of N_s by the volumetric concentration of carbon atoms in a graphite layer (37.9 atoms/nm^{-3}) and by using the literature values for the diffusion coefficient of carbon in iron at 1023 K (750 °C), $D = 3.2 \times 10^{-7}$ cm^2/s, volume of carbon atom $\Omega = 8.8 \times 10^{-3}$ nm^3, and the value of $r_o = 3.1$ nm from the TEM measurements. Under these assumptions we calculate the value of $G_D = 2.2 \times 10^5$ μm/min.

We can also estimate the parameter G_D using a slightly different argument. The atomic fraction of carbon in iron at equilibrium with graphite (and MWCNT), ΩN_0, could hardly exceed the maximum atomic fraction of C in austenite ($\sim 7 \times 10^{-2}$ at 1100 K). The equivalent fraction of carbon in a highly supersaturated solution, ΩN_0, should be noticeably higher. If we assume a supersaturation of 10 ($(N_s - N_0)/N_0 = 10$), and use the calculated carbon diffusivity in the BCC iron of 1.8×10^{-7} cm^2/s at 1100 K[28] (which is not far away from the value $D = 3.2 \times 10^{-7}$ cm^2/s used for the previous estimate) and the catalyst radius $R = 3.1$ nm, then we arrive at the estimate of $G_D = 2.4 \times 10^5$ μm/min, which is quite close to the value obtained from the previous estimate.

Best fits of eqs 6 and 7 to our kinetic data (Figure 3B) using the calculated value of $G_D = 2.2 \times 10^5$ μm/min show that our model reproduces the key feature of the growth process—the nearly constant array growth rate followed by an abrupt growth termination—over the whole range of the growth times. The value of the parameter obtained from the fit, $G_0 = 30.7$ μm/min, is indeed much smaller than the value of G_D, thus providing another consistency check for our model. Finally, we note that the exponential growth rate decay (dotted line in Figure 3B) does not describe the abrupt growth cessation observed in the experiment.

Growth Rate and the Total Process Pressure. The observed nonlinear dependence of the measured growth rate as a function of the total pressure (Figure 2A) could be rationalized by considering the ethylene/hydrogen balance in overall thermal decomposition reaction

$$C_2H_4 \leftrightarrow 2H_2 + 2C$$

At equilibrium, this reaction is described by the following balance of chemical potentials

$$\mu_{C_2H_4} = 2\mu_{H_2} + 2\mu_C \quad (8)$$

or

$$k_BT \ln \frac{P_{C_2H_4}}{P_{H_2}{}^2} = K = 2\mu_C + 2\mu_{H_2}{}^0 - \mu_{C_2H_4}{}^0$$

were the subscripts denote the chemical species, $\mu^o{}_i$ is the standard state chemical potential of the species *i*and *K* is the equilibrium constant. Away from equilibrium, the net carbon production per unit time per unit catalyst area, i.e., $2J_s$, is given by the difference between rate of the C_2H_4 decomposition and the reverse reaction rate. The decomposition occurs when an adsorbed C_2H_4 molecule overcomes the activation barrier E_a for decomposition; hence the chance to find the ethylene molecule in this exited state is $e^{(\mu(C_2H_4)-E_a)/kT}$. Similarly, the probability of the inverse reaction is given by $e^{(2\mu(C)+2\mu(H_2)-E_a)/kT}$. Since ethylene decomposition requires dissociation of a covalent bond, it is reasonable to expect that the activation energy for this process will be much higher than the adsorption energies for C_2H_4 and H_2; therefore it is reasonable to assume that the adsorbed ethylene and hydrogen molecules are in equilibrium with the gas phase and that the corresponding chemical potentials, $\mu_{C_2H_4}$ and μ_{H_2} are equal in the adsorbed and gaseous states. If the deviations from the equilibrium are not extreme, the pre-exponent frequency factors, ν, for

the direct and inverse reactions should be equal. Therefore the carbon production flux may be approximated as

$$2J_s = v e^{(\mu(C_2H_4)-E_a)/k_BT} - v e^{(2\mu(H_2)+2\mu(C)-E_a)/k_BT} = v e^{-E_a/k_BT}(e^{(\mu(C_2H_4)-2\mu(H_2)-2\mu(C))/k_BT} - 1)e^{(2\mu(H_2)+2\mu(C))/k_BT} \quad (9)$$

Finally, we can rewrite this equation as:

$$v_g \sim v e^{-E_a/k_BT} K P_{H_2}{}^2 \left(\frac{P_{C_2H_4}}{P_{H_2}{}^2 K} - 1 \right) = v e^{-E_a/k_BT}(\xi_{C_2H_4} P_0 - K \xi_{H_2}^2 P_0{}^2) \quad (10)$$

where the constants ξ_i denotes the volume fractions of a particular gas in the gas mixture. It is clear from the last two terms of the eq 10 that as the total pressure P_0 increases, the carbon production at first rises but then starts to decrease as the quadratic term starts to overwhelm the linear term. In other words, carbon production always increases proportionally to P_0, while carbon removal by hydrogen increases as $P_0{}^2$. The data do show a very similar trend with the variations of process pressure (Figure 2A). Finally, the observed decrease in the CNT growth rates with the increase of water concentration likely reflects the etching of both the amorphous carbon and the graphitic carbon. The presence of significant amounts of water in the reaction mixture introduces a more complicated set of reaction processes that our model does not capture at this point.

Reproducible growth of nanotube arrays under controlled conditions that we have demonstrated removes many obstacles to the technological applications of carbon nanotube arrays. Tight control over CNT array dimensions should enable their incorporation into the MEMS and NEMS devices using processes and architectures that require high reproducibility and close matching of the components. We also showed that the kinetics of CNT array growth can be described quantitatively using a simple model that considers carbon pyrolysis equilibrium, carbon diffusion through the catalyst particle, and poisoning of the catalyst surface. Further refinements to this model should lead to a better understanding and better control of CNT growth by thermal CVD.

Acknowledgment. S.S. acknowledges support from the USI program at LLNL, A.A. and H.G.P. acknowledge support from the LLNL SEGRF fellowship program. This work was partially supported by the DARPA MGA program, Office of Basic Energy Science (BES) Division of Materials Science and Engineering, CA State DWR grant, and the NSF NIRT Grant CBET-0709090. Parts of this work were performed under the auspices of the U.S. Department of Energy by Lawrence Livermore National Laboratory under Contract DE-AC52-07NA27344.

Supporting Information Available: Figures showing micro-Raman spectroscopy of the VA-CNT array and termination of growth, both macroscopic and microscopic behavior. This material is available free of charge via the Internet at http://pubs.acs.org.

References

(1) Fan, S. S.; Chapline, M. G.; Franklin, N. R.; Tombler, T. W.; Cassell, A. M.; Dai, H. J. Self-oriented regular arrays of carbon nanotubes and their field emission properties. *Science* **1999**, *283* (5401), 512–514.

(2) Niu, C. M.; Sichel, E. K.; Hoch, R.; Moy, D.; Tennent, H. High power electrochemical capacitors based on carbon nanotube electrodes. *Appl. Phys. Lett.* **1997**, *70* (11), 1480–1482.

(3) Saridara, C.; Mitra, S. Chromatography on self-assembled carbon nanotubes. *Anal. Chem.* **2005**, *77* (21), 7094–7097.

(4) Dai, H. J. Carbon nanotubes: synthesis, integration, and properties. *Acc. Chem. Res.* **2002**, *35* (12), 1035–1044.

(5) Holt, J. K.; Park, H. G.; Wang, Y.; Stadermann, M.; Artyukhin, A. B.; Grigoropoulos, C. P.; Noy, A.; Bakajin, O. Fast mass transport through sub-2-nanometer carbon nanotubes. *Science* **2006**, *312* (5776), 1034–1037.

(6) Hinds, B. J.; Chopra, N.; Rantell, T.; Andrews, R.; Gavalas, V.; Bachas, L. G. Aligned multiwalled carbon nanotube membranes. *Science* **2004**, *303* (5654), 62–65.

(7) Hafner, J. H.; Bronikowski, M. J.; Azamian, B. R.; Nikolaev, P.; Rinzler, A. G.; Colbert, D. T.; Smith, K. A.; Smalley, R. E. Catalytic growth of single-wall carbon nanotubes from metal particles. *Chem. Phys. Lett.* **1998**, *296* (1−2), 195–202.

(8) Puretzky, A. A.; Geohegan, D. B.; Jesse, S.; Ivanov, I. N.; Eres, G. In situ measurements and modeling of carbon nanotube array growth kinetics during chemical vapor deposition. *Appl. Phys. A: Mater. Sci. Process.* **2005**, *81* (2), 223–240.

(9) Christen, H. M.; Puretzky, A. A.; Cui, H.; Belay, K.; Fleming, P. H.; Geohegan, D. B.; Lowndes, D. H. Rapid growth of long, vertically aligned carbon nanotubes through efficient catalyst optimization using metal film gradients. *Nano Lett.* **2004**, *4* (10), 1939–1942.

(10) Kong, J.; Soh, H. T.; Cassell, A. M.; Quate, C. F.; Dai, H. J. Synthesis of individual single-walled carbon nanotubes on patterned silicon wafers. *Nature* **1998**, *395* (6705), 878–881.

(11) Delzeit, L.; Chen, B.; Cassell, A.; Stevens, R.; Nguyen, C.; Meyyappan, M. Multilayered metal catalysts for controlling the density of single-walled carbon nanotube growth. *Chem. Phys. Lett.* **2001**, *348* (5−6), 368–374.

(12) Su, M.; Zheng, B.; Liu, J. A scalable CVD method for the synthesis of single-walled carbon nanotubes with high catalyst productivity. *Chem. Phys. Lett.* **2000**, *322* (5), 321–326.

(13) Ci, L. J.; Xie, S. S.; Tang, D. S.; Yan, X. Q.; Li, Y. B.; Liu, Z. Q.; Zou, X. P.; Zhou, W. Y.; Wang, G. Controllable growth of single wall carbon nanotubes by pyrolizing acetylene on the floating iron catalysts. *Chem. Phys. Lett.* **2001**, *349* (3−4), 191–195.

(14) Futaba, D. N.; Hata, K.; Yamada, T.; Mizuno, K.; Yumura, M.; Iijima, S. Kinetics of water-assisted single-walled carbon nanotube synthesis revealed by a time-evolution analysis. *Phys. Rev. Lett.* **2005**, *95* (5), 056104−4.

(15) Meshot, E. R.; Hart, A. J. Abrupt self-termination of vertically aligned carbon nanotube growth. *Appl. Phys. Lett.* **2008**, *92*, 113107.

(16) Hata, K.; Futaba, D. N.; Mizuno, K.; Namai, T.; Yumura, M.; Iijima, S. Water-assisted highly efficient synthesis of impurity-free single-waited carbon nanotubes. *Science* **2004**, *306* (5700), 1362–1364.

(17) Puretzky, A. A.; Eres, G.; Rouleau, C. M.; Ivanov, I. N.; Geohegan, D. B. Real-time imaging of vertically aligned carbon nanotube array growth kinetics. *Nanotechnology* **2008**, *19* (5), 55605.

(18) Xiang, R.; Yang, Z.; Zhang, Q.; Luo, G.; Qian, W.; Wei, F.; Kadowaki, M.; Einarsson, E.; Maruyama, S. Growth deceleration of vertically aligned carbon nanotube arrays: catalyst deactivation or feedstock diffusion controlled. *J. Phys. Chem. C* **2008**, *112* (13), 4892–4896.

(19) Chernov, A. *Modern crystallography v.III: Crystal growth* Springer-Verlag: Berlin and New York, 1984; Vol. 36, p 517.

(20) Hata, K.; Futaba, D. N.; Mizuno, K.; Namai, T.; Yumura, M.; Iijima, S. Water-assisted highly efficient synthesis of impurity-free single-walled carbon nanotubes. *Science* **2004**, *306* (5700), 1362–1364.

(21) Helveg, S.; Lopez-Cartes, C.; Sehested, J.; Hansen, P. L.; Clausen, B. S.; Rostrup-Nielsen, J. R.; Abild-Pedersen, F.; Noerskov, J. K. Atomic-scale imaging of carbon nanofibre growth. *Nature* **2004**, *427* (6973), 426–429.

(22) Abild-Pedersen, F.; Norskov, J. K.; Rostrup-Nielsen, J. R.; Sehested, J.; Helveg, S. Mechanisms for catalytic carbon nanofiber growth studied by ab initio density functional theory calculations. *Phys. Rev. B* **2006**, *73* (11), 115419−13.

(23) Ci, L. J.; Manikoth, S. M.; Li, X. S.; Vajtai, R.; Ajayan, P. M. Ultrathick freestanding aligned carbon nanotube films. *Adv. Mater.* **2007**, *19* (20), 3300–3300.

(24) Johnson, W.; Mehl, R. Reaction kinetics in processes of nucleation and growth. *Trans. Am. Inst. Min., Metall. Pet. Eng.* **1939**, *135*, 416.
(25) Kolmogorov, A. On statistical theory of metal crystallisation. *Izv. Akad. Nauk SSSR, Ser. Mat.* **1937**, *3*, 355.
(26) Avrami, M. Granulation, phase change, and microstructure kinetics of phase change. III. *J. Chem. Phys.* **1941**, *9* (2), 177–184.
(27) Tibbetts, G. G.; Devour, M. G.; Rodda, E. J. An adsorption-diffusion isotherm and its application to the growth of carbon filaments on iron catalyst particles. *Carbon* **1987**, *25* (3), 367–375.
(28) Jiang, D. E.; Carter, E. A. Carbon dissolution and diffusion in ferrite and austenite from first principles. *Phys. Rev. B* **2003**, *67* (21), 214103.

NL803277G